Journal of Intelligent Systems and Control
https://www.acadlore.com/journals/JISC

Dynamic Characteristic Analysis of Tri-Stable Piezoelectric Energy Harvester with Double Elastic Amplifiers

Dawei Man[1,2*], Yingying Bai[1], Qingnan Hu[1], Huaiming Xu[1], Gaozheng Xu[1], Liping Tang[1,2]

[1] School of Civil Engineering, Anhui Jianzhu University, 230601 Hefei, China
[2] BIM Engineering Center of Anhui Province, 230601 Hefei, China

[*] Correspondence: Dawei Man (mandawei@ahjzu.edu.cn)

Received: 01-14-2023 **Revised:** 02-16-2023 **Accepted:** 03-01-2023

Citation: D. W. Man, Y. Y. Bai, Q. N. Hu, H. M. Xu, G. Z. Xu, and L. P. Tang, "Dynamic characteristic analysis of tri-stable piezoelectric energy harvester with double elastic amplifiers," *J. Intell Syst. Control*, vol. 2, no. 2, pp. 54-69, 2023. https://doi.org/10.56578/jisc020201.

Abstract: In order to further improve the vibration energy harvesting efficiency of piezoelectric energy harvester under low frequency environmental excitation, this paper, based on the traditional magnetic tri-stable piezoelectric energy collector model, proposes a tri-stable piezoelectric energy harvester (TPEH+DEM) model with two elastic amplifiers which are installed between the U-shaped frame and the base and between the fixed end of the piezoelectric cantilever beam and the U-shaped frame respectively. Based on Hamilton principle, the motion equation of electromechanical coupling of TPEH+DEM system is established, and the analytical solutions of displacement, output voltage and power of the system are obtained by harmonic balance method. The effects of the mass of elastic amplifier, spring stiffness, magnet spacing and load resistance on the dynamic characteristics of energy harvesting of TPEH+DEM system are analyzed. The result shows that there are two peaks in the response output power of TPEH+DEM system in the operating frequency range. By adjusting the mass and stiffness of the elastic amplifier reasonably, the system can move into the inter-well motion under low external excitation intensity, and produce high output power. Compared with the traditional model which only has an elastic amplifier on the base of piezoelectric energy harvester, TPEH+DEM model has better energy harvesting performance under low frequency and low intensity external excitation.

Keywords: Piezoelectric energy harvester; Electromechanical coupling; Elastic amplifier; Harmonic balance method; Inter-well motion

1. Introduction

Piezoelectric energy harvester can convert mechanical energy in the environment into electrical energy by using piezoelectric effect to supply power to microelectronic devices. The early linear piezoelectric energy harvester has a narrow working frequency band, so it is difficult to effectively match with the broadband vibration frequency in the environment, which leads to low energy harvesting efficiency [1-8]. To solve this problem, scholars at home and abroad begin to study the multi-stable piezoelectric energy harvester model to improve the energy harvesting performance of the system [9-16]. Chen et al. [17], based on the bi-stable piezoelectric energy harvesting model, analyzed the effects of material parameters, frequency and amplitude of external excitation on the system performance. Kim and Seok [18] studied a magnetic tri-stable piezoelectric cantilever beam energy harvester, and described in detail the advantages of tri-stable piezoelectric energy harvester for broadband vibration energy harvesting under low intensity excitation. Zhou et al. [19], based on the magnetic tri-stable piezoelectric energy harvester model, used numerical simulation and experimental method to demonstrate that the tri-stable piezoelectric energy harvester has better energy harvesting effect than bi-stable energy harvester under low external excitation level. Zhou and Zuo [20] obtained the analytical expression of steady-state response of asymmetric tri-stable piezoelectric cantilever beam by harmonic balance method, and analyzed the influence of potential well depth on energy harvesting effect under different excitation conditions.

At present, most of the studied multi-stable piezoelectric energy harvesters are fixed on rigid bases. Once the

positions of cantilever beams and magnets are fixed, it will be difficult to adjust the frequency bandwidth of piezoelectric harvesters to match the external excitation frequency by changing the relative positions between magnets, so as to realize large-scale inter-well motion [21-22]. Considering the above shortcomings of rigid base and to further improve the power output of multi-stable piezoelectric energy harvester under weak excitation intensity, researchers introduce elastic amplifier base into the structure of multi-stable piezoelectric energy harvester [23]. Liu et al. [24] proposed an elastic amplifier piezoelectric energy harvester with added mass, and demonstrated through experiments that the energy harvester can enhance vibration harvesting and reduce resonance frequency while broadening its operating frequency range. Wang et al. [25] demonstrated through numerical simulation and experimental method that the bi-stable piezoelectric energy harvester (BPEH+EM) system with elastic amplifier is easier to jump out of the barrier and move into large-scale inter-well motion at lower excitation level, and produces higher output power. Wang et al. [26] designed a piezoelectric cantilever beam energy harvester model with elastic amplifier, which provides enough kinetic energy to overcome the tri-stable potential well barrier, so that the system moves into large-scale well motion.

Based on the magnetic tri-stable piezoelectric cantilever beam energy harvester model with elastic amplifier base, a new type of amplifier composed of mass block M_f and spring k_f is added to the fixed end of the piezoelectric cantilever beam to form a TPEH+DEM model with double elastic amplifiers. Considering the eccentric distance and moment of inertia of the free end magnet of the beam, the motion control equation of electromechanical coupling of TPEH+DEM system is established based on Hamilton principle, and the analytical solution of the equation is obtained by using harmonic balance method. Focus is put on the effects of the relative position of magnet spacing, the mass and stiffness of elastic amplifier on the energy harvesting performance of TPEH+DEM system, and the calculation result of TPEH+DEM model is compared with that of traditional TPEH+EM model.

2. Modeling of Piezoelectric Energy Harvester

Figure 1 is a structural model of the TPEH+DEM with double elastic amplifiers established in this paper. TPEH consists of a cantilever piezoelectric beam of length l and width b and a beam-end magnet (expressed by A) and two external magnets (expressed by B and C) fixed to the right side of the U-shaped frame. The horizontal distance between the piezoelectric beam cantilever end magnet A and the U-shaped frame fixed magnet is d_h, and the vertical distance from the free end magnet of the beam to the external magnet B (external magnet C) is d_v. The cantilever beam consists of a metal substrate with a thickness of h_s and two piezoelectric patches with a thickness of t_p covering the upper and lower surfaces of the cantilever beam. The two piezoelectric patches have opposite polarization in the thickness direction and are connected in series with an external load resistor R. DEM consists of two elastic amplifiers (denoted EM_1 and EM_2), of which EM_1 comprises a U-shaped frame and a spring k_b between TPEH and the substrate; EM_2 consists of a spring k_f connecting the beam end mass M_f and the bottom of the U-shaped frame.

In Figure 1, $z(s, t)$, $z_m(t)$ and $z_b(t)$ represent the relative vertical displacement between a certain point on the section of piezoelectric cantilever beam and the fixed end of the beam, the vibration displacement of the U-shaped frame and the vertical vibration displacement of the base, respectively. The eccentric distance of the beam-end magnet is represented by e. Assuming that the metal substrate and the piezoelectric layer are completely tightly bonded, the constitutive relation is expressed as follows:

$$\left.\begin{aligned} T_1^{\mathrm{s}} &= Y_{\mathrm{s}} S_1^{\mathrm{s}} \\ T_1^{\mathrm{p}} &= Y_{\mathrm{p}} \left(S_1^{\mathrm{p}} - d_{31} E_3 \right) \\ D_3 &= d_{31} T_1 + \varepsilon_{33}^{\mathrm{T}} E_3 \end{aligned}\right\} \tag{1}$$

where, parameters related to the substrate are denoted by superscript s, and parameters related to the piezoelectric layer are denoted by subscript p; x and y directions are represented by 1 and 3 in subscripts, respectively; T, S, Y, D_3 and d_{31} denote the stress, strain, Young modulus, electric displacement, and piezoelectric constant of the piezoelectric cantilever beam, respectively; ε_{33}^{T} is the dielectric constant of the piezoelectric layer when the stress is constant; E_3=-$V(t)$/(2t_P), E represents electric field strength and $V(t)$ is voltage; the expression of the relationship between displacement and strain is $S_1^S = S_1^P = -yz''$, where y is the distance between the neutral axis of the piezoelectric cantilever beam and any point on its cross section, z'' is the curvature of the piezoelectric cantilever beam.

The Lagrange equation of the system is as follows:

$$\int_{t_1}^{t_2} \left[\delta(T_K + W_P - U_e - U_m - U_d) + \delta W \right] dt = 0 \tag{2}$$

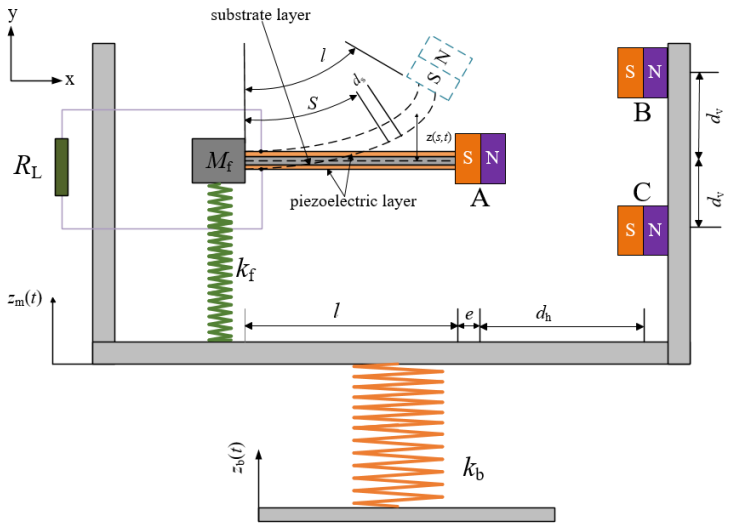

(a) (Front elevation of model)

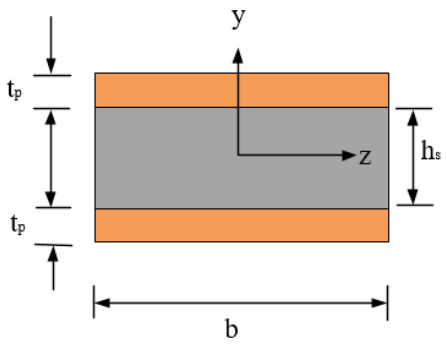

(b) Section map of model

Figure 1. Structural model of TPEH+DEM

where, T_k is kinetic energy, U_e is strain energy, W_p is electric potential energy of electric field, U_m is magnetic potential energy between magnets, U_d is elastic potential energy, and W is external work. Their expressions are as follows.

$$\begin{aligned} T_k &= \frac{1}{2}\int_0^l m(\dot{z}+\dot{z}_m(t))^2 ds + \frac{1}{2}M_t\left(\dot{z}(l,t)+e\dot{z}'(l,t)+\dot{z}_m(t)\right)^2 \\ &+\frac{1}{2}J\dot{z}'(l,t)^2+\frac{1}{2}M_f(\dot{z}(0,t)+\dot{z}_m(t))^2+\frac{1}{2}M_m\dot{z}_m(t)^2 \end{aligned} \tag{3}$$

where, $z(l, t)$ is the displacement of the piezoelectric cantilever beam at $s=l$; $m=2\rho_p t_p b+\rho_s h_s b$ is the equivalent mass on the unit beam, where ρ_p is the density of the piezoelectric layer and ρ_s is the density of the substrate; the mass, eccentric distance and moment of inertia of free end magnet A of the piezoelectric cantilever beam are represented by M_t, e and J, respectively; $(\dot{})$ denotes the derivative of time t.

$$U_e = \frac{1}{2}\int_0^l \left[YIz''^2 - Y_p b d_{31}\left(h+\frac{t_p}{2}\right)Z(t)z'' \right] ds \tag{4}$$

where,

$$h = h_s/2,\ YI = Y_s I_s + Y_p I_p\ YI = \frac{2}{3}[Y_s bh^3 + Y_p b(3h^2 t_p + 3ht_p{}^2 + t_p{}^3)] \tag{5}$$

$$W_P = \frac{1}{2}Y_p b d_{31}(\mathrm{h}+\frac{t_p}{2})V(t)\int_0^l z''ds + bl\varepsilon_{33}^S \frac{V(t)^2}{4t_p} \tag{6}$$

$$U_d = \frac{1}{2}k_f z(0,t)^2 + \frac{1}{2}k_b z_m{}^2 \tag{7}$$

$$\begin{aligned}\delta W &= \delta z_m \ddot{z}_b (M_m + M_t + ml + M_f) \\ &+\delta X(t)\ddot{z}_b \left(M_t\varphi_1(l) + m\int_0^l \varphi_1(s)ds + M_t e\varphi_1'(l) + M_f\varphi_1(0)\right)\end{aligned} \tag{8}$$

where, $\varepsilon_{33}^S = \varepsilon_{33}^T - d_{31}^2 Y_p$, ε_{33}^S is the dielectric constant of the piezoelectric layer when the stress is constant.

According to the magnetic dipole model [27, 28] after considering eccentric distance at the free end magnet of the beam, it can be obtained that:

$$\begin{aligned}U_{\mathrm{m}} = \frac{\mu_0}{4\pi}\Bigg[&\frac{\mathbf{m}_{\mathrm{B}}}{\|\mathbf{r}_{\mathrm{BA}}\|_2^3} + \frac{\mathbf{m}_{\mathrm{C}}}{\|\mathbf{r}_{\mathrm{CA}}\|_2^3} - \frac{(\mathbf{m}_{\mathrm{B}}\cdot\mathbf{r}_{\mathrm{BA}})3\mathbf{r}_{\mathrm{BA}}}{\|\mathbf{r}_{\mathrm{BA}}\|_2^5} \\ &- \frac{(\mathbf{m}_{\mathrm{C}}\cdot\mathbf{r}_{\mathrm{CA}})3\mathbf{r}_{\mathrm{CA}}}{\|\mathbf{r}_{\mathrm{CA}}\|_2^5}\Bigg]\cdot\mathbf{m}_{\mathrm{A}}\end{aligned} \tag{9}$$

where, $\mu_0 = 4\pi\times10^{-7} H\cdot m^{-1}$ indicates vacuum magnetic conductivity,

$$\begin{aligned}\mathbf{r}_{\mathrm{BA}} &= \left[-d_{\mathrm{h}} - \Delta x \quad v(l,t) + e\sin\beta - d_{\mathrm{v1}}\right], \\ \mathbf{r}_{\mathrm{CA}} &= \left[-d_{\mathrm{h}} - \Delta x \quad v(l,t) + e\sin\beta + d_{\mathrm{v2}}\right],\end{aligned}$$

The magnetic dipole moments are $\mathbf{m}_A$=[$M_AV_A cos\beta$ $M_AV_A sin\beta$], $\mathbf{m}_B$=[$-M_BV_B$ 0] and $\mathbf{m}_C$=[$-M_CV_C$ 0]. In $\Delta x \approx e(1-cos\beta)$, $\beta = arctan v'(l)$, M_A, M_B and M_C are the magnetization intensity of magnets A, B and C, respectively, and V_A, V_B and V_C are the volumes of magnets A, B and C, respectively.

Using Galerkin method, the displacement $z(s, t)$ is expressed as:

$$z(s,t) = \phi_r(s)X_r(t) \tag{10}$$

where, $X_r(t)$ is the r-th modal coordinate of the piezoelectric cantilever beam, $\phi_r(s)$ represents the r-th modal function of the beam, and its normalized condition expression is:

$$\begin{aligned}&\int_0^l \varphi_s(s)m\varphi_r(s)ds + \varphi_s(l)M_t\varphi_r(l) + \varphi_s(l)M_t e\varphi_r'(l) \\ &+\varphi_s(0)M_f\varphi_r(0) + \varphi_s'(l)(J + M_t e^2)\varphi_r'(l) \\ &+\varphi_s'(l)M_t e\varphi_r(l) = \delta_{rs}\end{aligned} \tag{11}$$

$$\int_0^l \frac{d^2\varphi_s(s)}{ds^2} YI \frac{d^2\varphi_r(s)}{ds^2} ds + \varphi_s(0)k_f\varphi_r(0) = \omega_r{}^2\delta_{rs} \tag{12}$$

where, δ_{rs} is the Kronecker function. When $s=r$, δ_{rs} is 1; when $s\neq r$, δ_{rs} is 0. The expression of inherent frequency of the piezoelectric cantilever beam under undamped vibration is $\omega_r = \lambda_r^2\sqrt{YI/(ml^4)}$, where λ_r is its eigen value. The calculation method of λ_r and vibration mode function can be seen in reference [18].

Considering only the first-order mode and substituting formula (10) into formula (9), this paper expands at $X_1(t)$=0 by using Taylor's formula and can obtain:

$$\begin{aligned}U_m &= k_0 - \frac{1}{2}k_1 X_1{}^2 + \frac{1}{4}k_2 X_1{}^4 + \frac{1}{6}k_3 X_1{}^6 \\ &+o(X_1{}^7)\end{aligned} \tag{13}$$

where,

$$k_0 = \frac{2kq_1}{\left(d_h{}^2 + d_v{}^2\right)^2},$$

$$k_1 = \frac{4k}{\left(d_h^{\,2} + d_v^{\,2}\right)^{5/2}}\left[q_1\left(2.5q_2 - 17.5q_3^{\,2}\right) - 5q_3q_4\left(d_h^{\,2} + d_v^{\,2}\right) - q_5\right]$$

$$k_2 = \frac{8k}{\left(d_h^{\,2} + d_v^{\,2}\right)^{5/2}}[q_1(-2.5q_6 - 17.5q_3q_7 + 4.38q_2^{\,2} - 78.75q_2q_3^{\,2} + 144.375q_3^{\,4}) + q_4(-2.5q_7 - 17.5q_2q_3 + 52.5q_3^{\,3}\left(d_h^{\,2} + d_v^{\,2}\right) q_5\left(-2.5q_2 + 17.5q_3^{\,2}\right) + 5q_3q_8 + q_9]$$

$$k_3 = \frac{12k}{\left(d_h^{\,2} + d_v^{\,2}\right)^{5/2}}[q_1(-2.5q_{10} + 13.125q_3q_{11} + 8.75q_2q_6 + 4.375q_7^{\,2} - 78.78q_3^{\,2}q_6 + 78.25q_2q_3q_7 - 288.75q_3^{\,3}q_7 + 216.55q_2^{\,2}q_3^{\,2} - 6.56q_2^{\,3} - 938.44q_2q_3^{\,4} + 938.44q_3^{\,6}) + q_4(1.875q_{11} - 17.5q_3q_6 + 8.75q_2q_7 - 78.75q_3^{\,2}q_7 + 39.38q_2^{\,2}q_3 - 288.75q_2q_3^{\,2} + 375.375q_3^{\,5}) + q_5(-2.5q_6 - 17.5q_3q_7 + 4.375q_2^{\,2} - 78.75q_2q_3^{\,2} + 144.375q_3^{\,4}) + q_8(-2.5q_7 - 17.5q_2q_3 + 52.5q_3^{\,2}) + q_9(-2.5q_2 + 17.5q_3^{\,2}) + 5q_3q_{12} + q_{13}]$$

Coefficient κ, the expression of $q_{i=1\ldots26}$ is shown in the previous reference [18].

Considering only the first-order mode, formula (2) is substituted into the Lagrange variational equation shown in formula (14):

$$\begin{cases} \dfrac{d}{dt}\left(\dfrac{\partial L}{\partial \dot{z}_m}\right) - \dfrac{\partial L}{\partial z_m} + \dfrac{\partial W}{\partial z_m} = 0 \\ \dfrac{d}{dt}\left(\dfrac{\partial L}{\partial \dot{X}}\right) - \dfrac{\partial L}{\partial X} + \dfrac{\partial W}{\partial X} = F(t) \\ \dfrac{d}{dt}\left(\dfrac{\partial L}{\partial \dot{V}}\right) - \dfrac{\partial L}{\partial V} + \dfrac{\partial W}{\partial V} = Q(t) \end{cases} \tag{14}$$

where, $F(t) = -2\xi_1\omega_1\dot{\eta}_1(t)$ is the generalized dissipative force of TPEH+DEM system, ω_1 is the first-order natural frequency of the system, ξ_1 is its damping ratio and $Q(t)$ is generalized output charge. $\dot{Q}(t) = -V(t)/R$, where R represents the load resistance of external circuit. Through formula (14), the differential equation of motion of TPEH+DEM system can be obtained as follows:

$$\begin{cases} M_0\ddot{X}_1(t) + M_1\ddot{z}_m(t) + k_b z_m = -M_1\ddot{z}_b(t) \\ \ddot{X}_1(t) + 2\xi_1\omega_1\dot{X}_1(t) + \omega_1^{\,2}X_1(t) - k_1X_1(t) \\ \quad + k_2X_1(t)^3 + k_3X_1(t)^5 - \theta_1V(t) \\ \quad + M_0\ddot{z}_m(t) = -M_0\ddot{z}_b(t) \\ C_P\dot{V}(t) + \dfrac{V(t)}{R} + \theta_1\dot{X}_1(t) = 0 \end{cases} \tag{15}$$

where,

$$M_0 = m\int_o^l \phi_1(s)ds + M_t\phi_1(l) + M_t e\phi_1'(l) + M_f\phi_1(0), \quad M_1 = ml + M_t + M_f + M_m,$$

$$\omega_1^{\,2} = YI\int_0^l \phi_1''(s)^2 ds + k_f \phi_1(0)^2 \,,\ \theta_1 = Y_P b d_{31}\left(h+\frac{t_P}{2}\right)\int_0^l \phi_1''(s)ds \,,\ C_P = \frac{bl\varepsilon_{33}^S}{2t_P}\,.$$

where,

$$\omega_1^2 = YI\int_0^l \varphi_1''\,ds,\ g_0 = mg\int_0^l \varphi_1(s)ds$$
$$+M_t g\varphi_1(l)\,,\ \Gamma_1 = m\int_0^l \varphi_1(s)ds + M_{\mathrm{t}}\left(\varphi_1(l)+e\varphi_1'(l)\right)$$
$$\theta_1 = Y_P b d_{31}\left(h+\frac{t_P}{2}\right)\int_0^l \varphi_1(s)ds\,,\ C_P = \frac{bl\varepsilon_{33}^S}{2t_P}\,.$$

External excitation is set to $\ddot{v}_b(t) = \bar{v}_b\, cos(\,\omega_e t)$, where $\bar{v}_b$ is the amplitude of external excitation, ω_e is the circular frequency of excitation. Substituting dimensionless transformation $x=\eta_1/l$, $\bar{V} = VC_p/(l\theta_1)$ and $\tau=\omega_1 t$ into formula (15), we can get

$$\begin{cases} M_0\ddot{x} + M_1\ddot{V}_{\mathrm{m}} + K_{\mathrm{b}}V_{\mathrm{m}} = -M_1\ddot{V}_{\mathrm{b}} \\ \ddot{x} + 2\xi_1\dot{x} + (1-K_1)x + K_2x^3 + K_3x^5 \\ -\Theta\bar{V} + M_0\ddot{V}_{\mathrm{m}} = -M_0\ddot{V}_{\mathrm{b}} \\ \dot{\bar{V}} + \alpha\bar{V} + \dot{x} = 0 \end{cases} \tag{16}$$

where, $K_b = \frac{k_b}{{\omega_1}^2}$, $K_1 = \frac{k_1}{{\omega_1}^2}$, $K_2 = \frac{k_2 l^2}{{\omega_1}^2}$, $\Theta = \frac{{\theta_1}^2}{C_P{\omega_1}^2}$, $\alpha = \frac{1}{C_P R_L \omega_1}$, $F = -\frac{M_0\bar{z}_b}{{\omega_1}^2 l}$.

The first and second equations of formula (16) are used to eliminate the variable V_{m}, and formula (16) is simplified to

$$\begin{cases} \dfrac{M_1 - {M_0}^2}{K_b}x^{(4)} + \dfrac{2M_1\xi_1}{K_b}x^{(3)} + \dfrac{M_1(1-K_1)+K_b}{K_b}\ddot{x} \\ +2\xi_1\dot{x} + (1-K_1)x + K_2x^3 + K_3x^5 + \dfrac{M_1K_2}{K_b}(6x\dot{x}^2 + 3x^2\ddot{x}) \\ +\dfrac{M_1K_3}{K_b}(20x^3\dot{x}^2 + 5x^4\ddot{x}) - \dfrac{M_1\Theta}{K_b}\ddot{\bar{V}} - \Theta\bar{V} = F\cos(\omega t) \\ \dot{\bar{V}} + \alpha\bar{V} + \dot{x} = 0 \end{cases} \tag{17}$$

3. Solution by Harmonic Balance Method

It is assumed that the solution of formula (17) can be expressed as:

$$\begin{cases} x = A(\tau)\sin(\omega\tau) + B(\tau)\cos(\omega\tau) \\ \bar{V} = C(\tau)\sin(\omega\tau) + D(\tau)\cos(\omega\tau) \end{cases} \tag{18}$$

where A, B, C and D are uncertain coefficients, the displacement amplitude of the piezoelectric cantilever beam can be expressed as $a=\sqrt{A^2+B^2}$, and the output voltage amplitude can be expressed as $u=\sqrt{C^2+D^2}$. We substitute formula (18) into formula (17), take the constant terms on both sides, and the coefficients of $\cos(\omega\tau)$ and $\sin(\omega\tau)$ are equal, and ignore the higher-order harmonic term, then the following equation is obtained:

$$\Pi_1(\ddot{B} - 2\omega\dot{A}) + 2\xi_1\dot{B} + \Pi_3 B - \Pi_2 A + \Pi_4 D - F = 0 \tag{19}$$

$$\Pi_1(\ddot{A} - 2\omega\dot{B}) + 2\xi_1\dot{A} + \Pi_2 B + \Pi_3 A + \Pi_4 C = 0 \tag{20}$$

$$\dot{C} - \omega D + \alpha C + \dot{A} - \omega B = 0 \tag{21}$$

$$\dot{D}+\omega C+\alpha D+\dot{B}+\omega A=0 \tag{22}$$

where,

$$\Pi_1=\frac{K_1M_1+K_b}{K_b}$$

$$\Pi_2=\frac{2\xi_1M_1}{K_b}\omega^3-2\xi_1\omega,$$

$$\Pi_3=\frac{M_1-M_0{}^2}{K_b}\omega^4-\frac{(1-K_1)M_1+K_b}{K_b}\omega^2+1-K_1$$

$$+\frac{3}{4}K_2a^2+\frac{5}{8}K_3a^4-\frac{3}{4}\frac{K_2M_1}{K_b}\omega^2a^2-\frac{5}{8}\frac{K_3M_1}{K_b}\omega^4a^4$$

$$\Pi_4=\frac{\Theta M_1}{K_b}\omega^2-\Theta$$

In the steady state, all derivatives of time are 0. Therefore, the analytical expressions of displacement amplitude and voltage amplitude of the system can be obtained by using formulas (19-22) as follows:

$$a^2\left[\left(\Pi_2+\Pi_4\frac{\alpha\omega}{\omega^2+\alpha^2}\right)^2+\left(\Pi_3-\Pi_4\frac{\omega^2}{\omega^2+\alpha^2}\right)^2\right]=F^2 \tag{23}$$

The steady-state displacement amplitude a of TPEH+DEM system can be calculated by formula (23). The expressions of steady-state output voltage and power amplitude are:

$$u=\left(\frac{\omega}{\sqrt{\omega^2+\alpha^2}}\right)a \tag{24}$$

$$P=\frac{l^2\theta_1{}^2u^2}{C_P{}^2R} \tag{25}$$

4. Analysis of Calculation Result

In this chapter, focus will be put on the effects of relative position of magnets, load resistance, mass of elastic amplifier and spring stiffness ratio on the performance of TPEH+DEM (Table 1). The main physical and geometric parameters of the system are as follows [1].

Table 1. The geometric and material properties of the TPEH+DEM

Parameter	Value
Length l	75mm
Width b	20mm
Thickness $\boldsymbol{h}_s$	0.2mm
Piezoelectric modulus $\boldsymbol{Y}_s$	70Gpa
Piezoelectric modulus $\boldsymbol{Y}_p$	60.98Gpa
Density ρ_s	2700kg/mm^3
Density ρ_p	7750kg/mm^3
Piezoelectric constant d_{31}	$-1.7\times10^{-10}C/N$
Permittivity of free space ε_{33}^S	$1.33\times10^{-8}F/m$
Damping ratio ξ_1	0.01
Magnetization of magnets (A,B,C)	$1\times10^{-6}m^3$
Volume of magnet (A,B,C)	$1.22\times10^{-6}m^3$
Eccentricity e	5mm
Mass of tip magnet M_t	14.9g

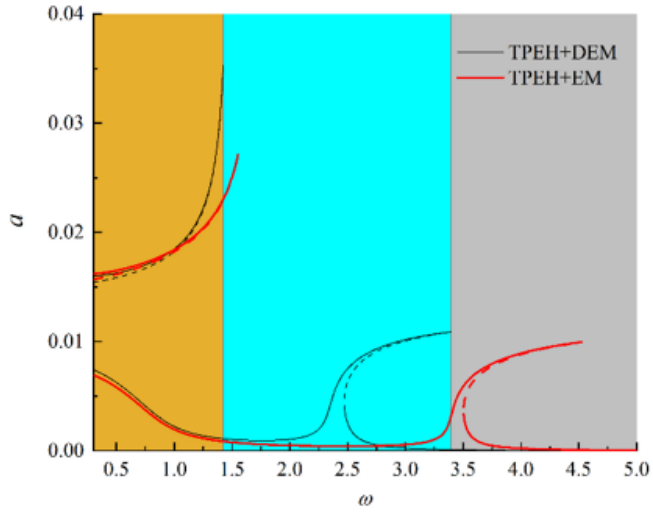

Figure 2. Variation curves of displacement amplitude of the system with excitation frequency under different models

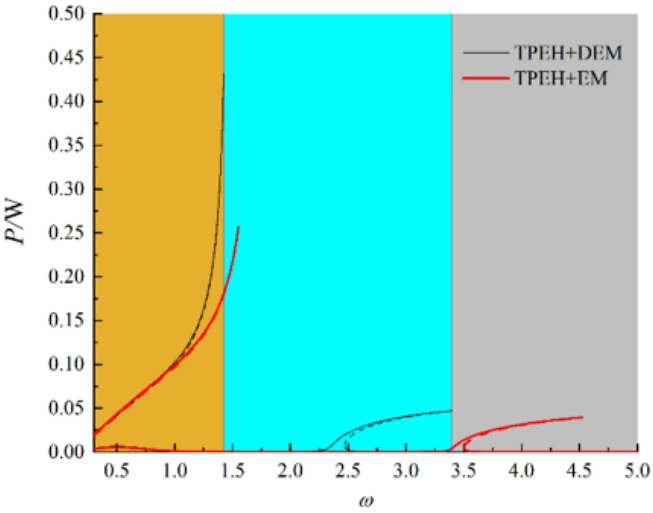

Figure 3. Variation curves of output power amplitude of the system with excitation frequency under different models

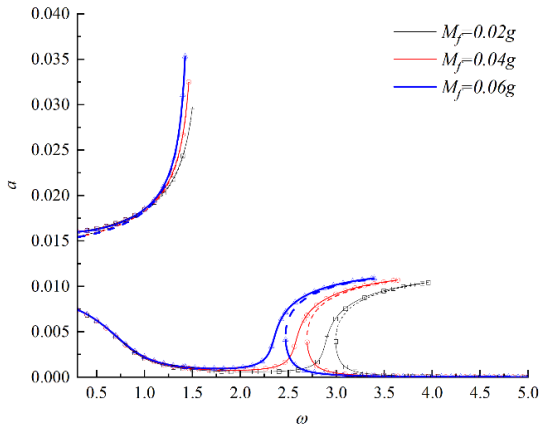

Figure 4. Variation curves of displacement amplitude of the system with excitation frequency in different values of M_f

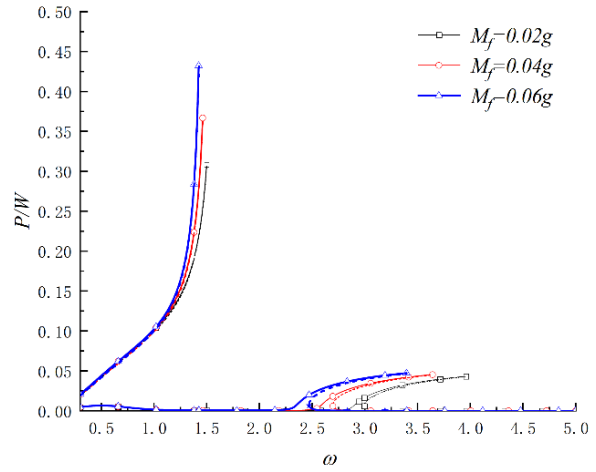

Figure 5. Variation curves of output power amplitude of the system with excitation frequency in different values of M_f

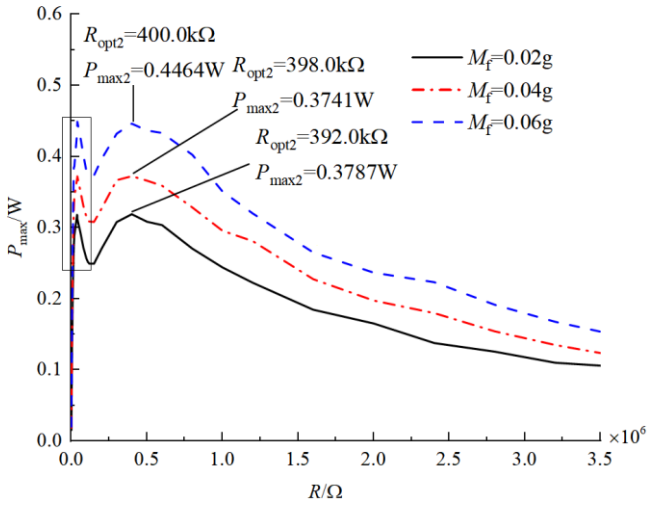

(a)

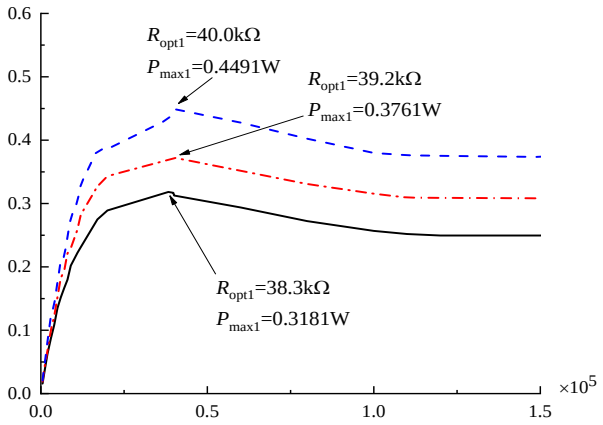

(b)

Figure 6. Variation curves of left peak power of the system with load resistance in different values of M_f

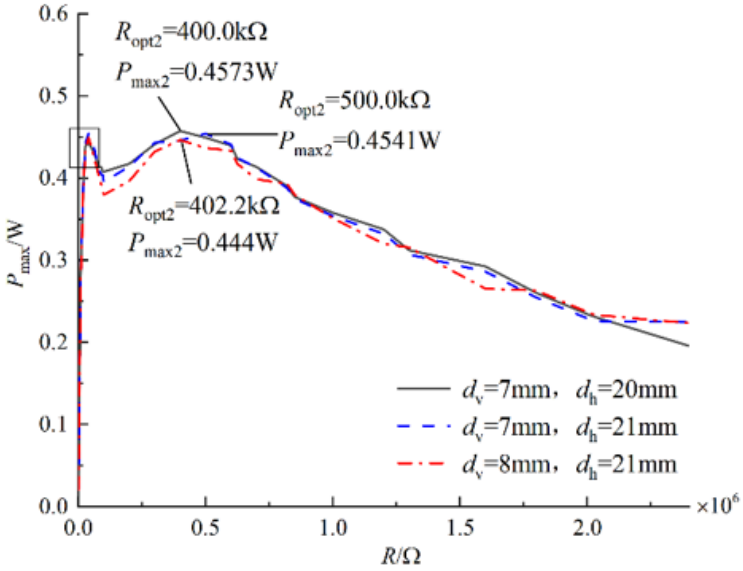

(a)

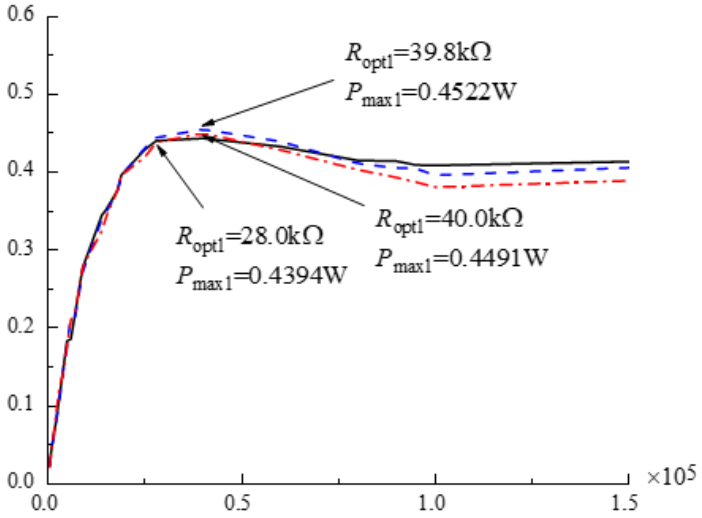

(b)

Figure 7. Variation curves of right peak power of the system with load resistance in different values of M_f

We take M_m=60 g, d_h=21 mm, d_v=8 mm and k_b=8,000 N/mm. The variation curves of displacement and output power amplitudes of the two models of piezoelectric energy harvester models (TPEH+DEM, TPEH+EM) with excitation frequency are shown in Figure 2 and Figure 3, respectively. TPEH+EM is equipped with only an elastic amplifier, i.e. a spring k_b located between TPEH and the substrate.

We take M_m=60 g, d_h=21 mm, d_v=8 mm, k_f=50,000 N/mm and k_b=8,000 N/mm. Figure 4 and Figure 5 show the variation curves of displacement amplitude a and power amplitude P of TPEH+DEM system with excitation frequency in different values of M_f s, respectively. As can be seen from Figure 4 and Figure 5, with the increase of M_f, left displacement and power peak of the system increase continuously, while right displacement and power peak change little, but the frequency band range moves to the low frequency band.

Figure 6 and Figure 7 show the variation curves of left and right peak power of TPEH+DEM system with load resistance R in different values of M_f when M_m=60 g, d_v=8 mm, d_h=21 mm, k_f=50,000 N/mm and k_b=8,000 N/mm. It can be seen from Figure 6 that with the increase of R, left peak power of the system increases rapidly first, and the first local maximum P_{max1} appears, corresponding to the load resistance R_{opt1}, and then continues to increase after greatly decreasing (when the load resistance is R_{opt2}, it reaches the second local maximum P_{max2} of the curve, and finally decreases gradually). In addition, it can be seen from Figure 6 that under the same M_f, the two local maxima are very close, and increasing M_f can obviously improve P_{max1} and P_{max2}. As shown in Figure 7, when M_f = 0.02g, left peak power of the system is 0.1130 W; when M_f increases to 0.06 g, right peak power of the system is 0.1115 W, that is, with the change of M_f, the peak power changes little.

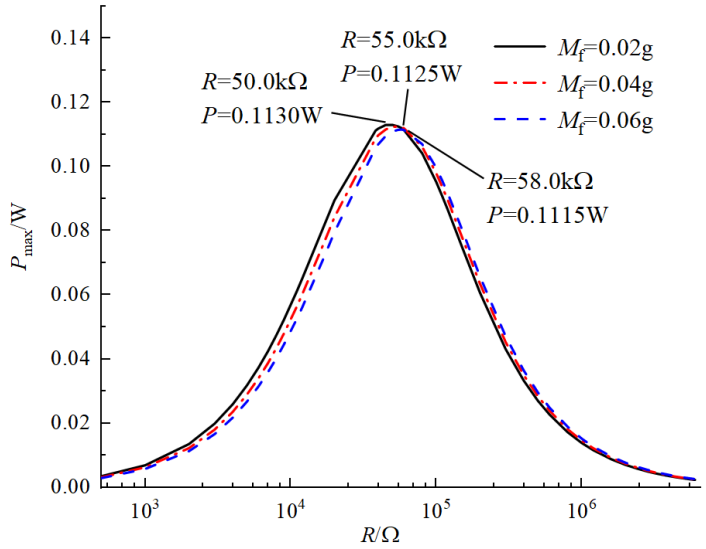

Figure 8. Variation curves of left peak power of the system with load resistance in different values of d_v and d_h

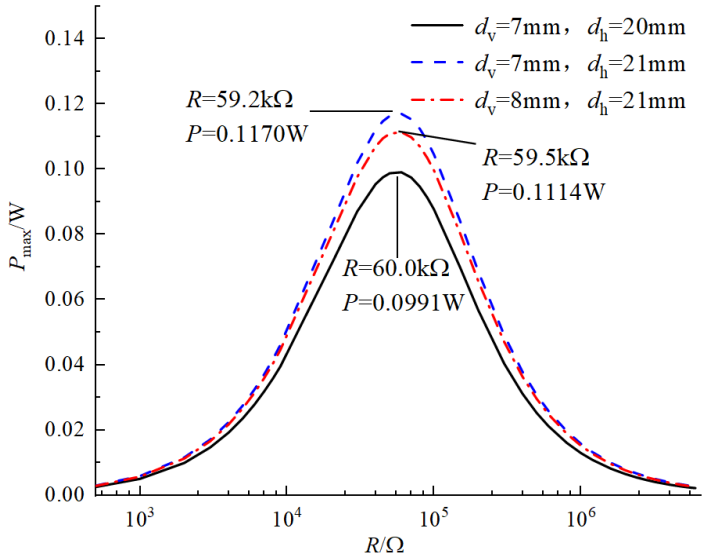

Figure 9. Variation curves of right peak power of the system with load resistance in different values of d_v and d_h

We take M_f=60 g, M_m=60 g, k_f=50,000 N/mm and k_b=8,000 N/mm. Figure 8 and Figure 9 show the variation curves of left and right peak power of TPEH+DEM system corresponding to different relative positions between magnets with load resistance R. As can be seen from Figure 8, the variation trend of left peak power of the system with load resistance R is the same as that of Figure 6, and the peak power of the system corresponding to different d_v and d_h is relatively close. Figure 9 shows that the peak power of the system can be significantly increased by increasing d_h while keeping dv constant. However, when d_h is kept constant, the peak power decreases slightly with the increase of d_v.

We take k_f=50,000 N/mm, k_b=8,000 N/mm, d_v=8 mm and d_h=21 mm. Figure 10 and Figure 11 show the variation curves of steady-state voltage amplitude u with excitation acceleration $\tilde{v}_b$ when ω is 0.8 and 1.2 respectively, and the mass of elastic amplifier is taken for different values. As can be seen from Figures 10 and 11, each working condition corresponds to an excitation acceleration threshold, which enables the system to move into large-scale inter-well motion and generate high output voltage. When ω is the same, the threshold of excitation acceleration required for the system to move into inter-well motion can be reduced by increasing the mass M_f and M_m of two elastic amplifiers, but the change of output voltage is not obvious. When the mass of elastic amplifiers is constant, the threshold of excitation acceleration increases with the increase of excitation frequency.

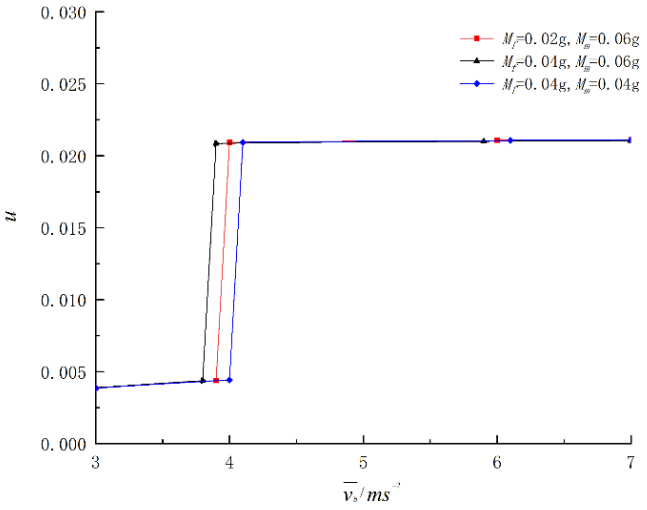

Figure 10. Variation curves of output voltage with excitation amplitude in different values of M_f and M_m when ω=0.8

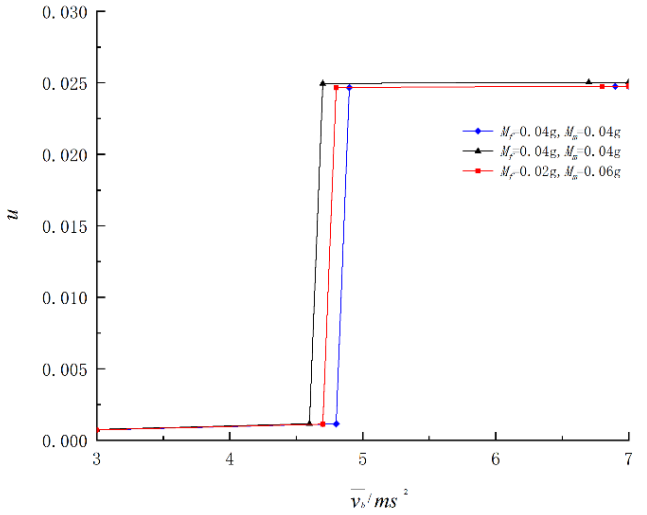

Figure 11. Variation curves of output voltage with excitation amplitude in different values of M_f and M_m when ω=1.2

Taking the load resistance R=300 kΩ, as shown in Figures 12 and 13, the steady-state voltage amplitude u of TPEH+DEM system varies with the excitation amplitude $\bar{v}_b$ when the excitation acceleration ω is 0.6 and 1.2, respectively and k_f/k_b is in different values. As shown in Figures 12 and 13, when ω=0.6, with the increase of k_f/k_b, the excitation threshold of the system decreases, while the steady-state voltage amplitude u changes little. When ω is increased to 1.2, the excitation threshold obviously decreases with the increase of k_f/k_b, and the output voltage amplitude increases with the increase of k_f/k_b after moving into inter-well motion. It can be seen that when the excitation frequency is high, increasing the k_f/k_b value can make the system move into inter-well motion and produce higher output voltage at lower excitation intensity.

Figures 14 and 15 show the variation curves of power and displacement amplitudes of the system when M_m is different in values and when R=300 kΩ, M_f=60 g, d_h=21, d_v=8, k_f=50,000 N/mm and k_b=50,000 N/mm. The result shows that, with the increase of excitation frequency, the power and displacement amplitudes of the system increase significantly at first, then decrease sharply after reaching the maximum value rapidly, then increase again, and then decrease after reaching the second local peak value when M_m keeps constant. In addition, with the increase

of M_m, the peak power and displacement of the system increase significantly, and can enter the secondary ascending section at lower excitation frequency, resulting in higher local peak power.

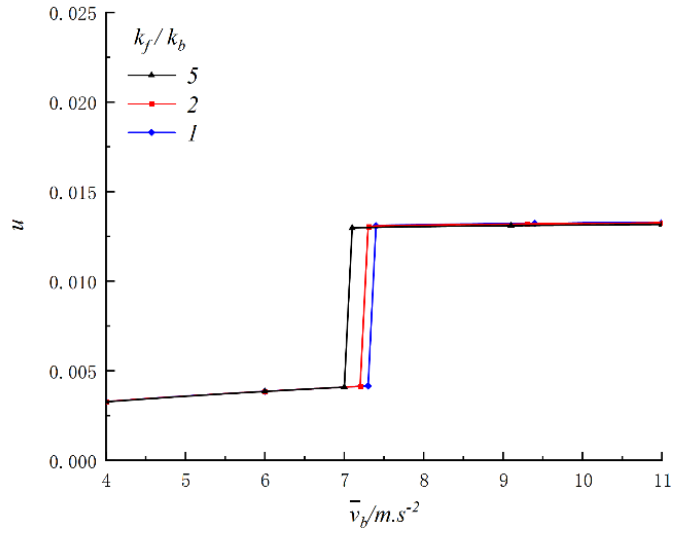

Figure 12. Variation curves of output voltage with excitation amplitude in different values of k_f/k_b when ω=0.6

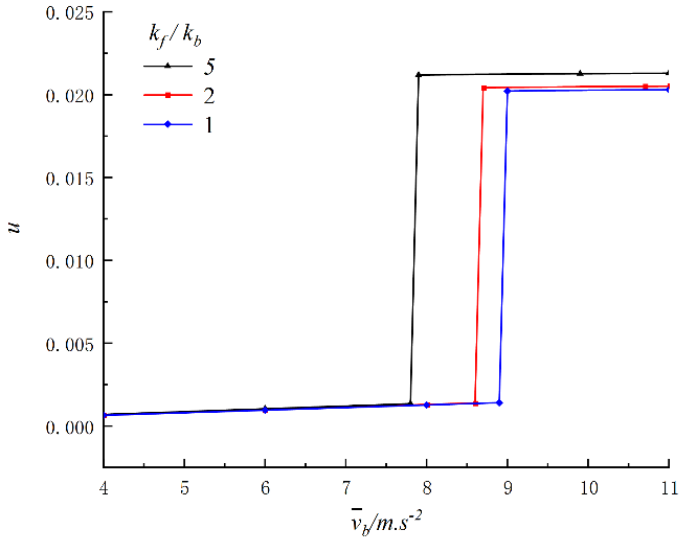

Figure 13. Variation curves of output voltage with excitation amplitude in different values of k_f/k_b when ω=1.2

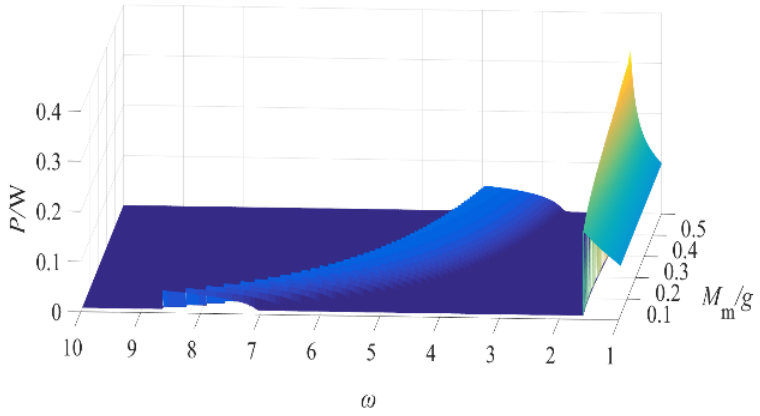

Figure 14. Curves of power amplitude changing with frequency in different values of M_m

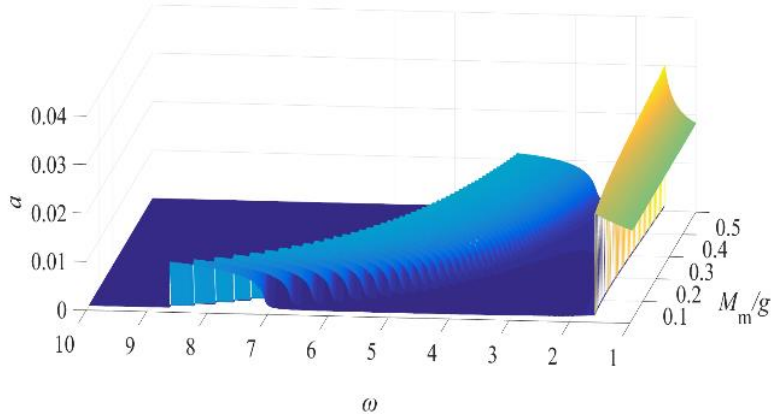

Figure 15. Curves of displacement amplitude changing with excitation frequency in different values of M_m

5. Conclusion

(1) Based on Hamilton variational principle, the differential equation of motion of a tri-stable piezoelectric energy harvesting system with double elastic amplifiers is derived, and the analytical solution of electromechanical coupling equation describing the energy output characteristics of the system is obtained by using the harmonic balance method.

(2) With the increase of excitation frequency, the output power amplitude of TPEH+DEM system can produce two high and low peaks. Compared with TPEH+EM system, TPEH+DEM system has better energy harvesting performance under low frequency external excitation.

(3) At the same excitation frequency, the excitation acceleration threshold required for TPEH+DEM system to move into inter-well motion can be reduced by increasing the mass of elastic amplifiers; when the excitation frequency is high, increasing the stiffness ratio k_f/k_b of the two elastic amplifiers can make TPEH+DEM system move into inter-well motion at lower excitation intensity and produce higher output voltage.

(4) Increasing M_m can significantly improve the maximum peak power of TPEH+DEM system, and can make the system enter the secondary ascending section at lower excitation frequency, resulting in higher local peak power.

Funding

This research was funded by the Anhui Provincial University Provincial Natural Science Research Project-Key Project (Grant No.: 2022AH050240); Doctoral Startup Foundation of Anhui Jianzhu University (Grant No.: 2020QDZ07); Scientific research Project of Anhui Education Department- Key Project (Grant No.: KJ2021JD01); Anhui Provincial Natural Science Foundation (Grant No.: 2108085MA28).

Data Availability

The data used to support the findings of this study are available from the corresponding author upon request.

Conflicts of Interest

The authors declare that they have no conflicts of interest.

References

[1] A. Erturk and D. J. Inman, "Broadband piezoelectric power generation on high-energy orbits of the bistable Duffing oscillator with electromechanical coupling," *J. Sound Vib.*, vol. 330, no. 10, pp. 2339-2353, 2011. https://doi.org/10.1016/j.jsv.2010.11.018.

[2] A. Erturk and D. J. Inman, "An experimentally validated bimorph cantilever model forpiezoelectric energy harvesting from base excitations," *Smart Mater. Struct.*, vol. 18, no. 2, Article ID: 025009, 2009. https://doi.org/10.1088/0964-1726/18/2/025009.

[3] A. Erturk, "Electromechanical modeling of piezoelectric energy harvesters," Doctoral Dissertation, Virginia Polytechnic Institute and State University, U.S.A., 2009.

[4] M. Safaei, H. A. Sodano, and R. Anton, "A review of energy harvesting using piezoelectric materials: State-of-the-art a decade later (2008-2018)," *Smart Mater. Struct.*, vol. 28, no. 11, Article ID: 113001, 2019. https://doi.org/10.1088/1361-665X/ab36e4.

[5] S. T. Fang, K. Y. Chen, J. T. Xing, S. X. Zhou, and W. H. Liao, "Tuned bistable nonlinear energy sink for simultaneously improved vibration suppression and energy harvesting," *Int J. Mech Sci.*, vol. 212, Article ID: 106838, 2012. https://doi.org/10.1016/j.ijmecsci.2021.106838.

[6] S. X. Zhou, M. Lallart, and A. Erturk, "Multistable vibration energy harvesters: Principle, progress, and perspectives," *J. Sound Vib.*, vol. 528, Article ID: 116886, 2022. https://doi.org/10.1016/j.jsv.2022.116886.

[7] K. Q. Fan, M. L. Cai, H. Y. Liu, and Y. W. Zhang, "Capturing energy from ultra-low frequency vibrations and human motion through a monostable electromagnetic energy harvester," *Energy*, vol. 169, pp. 356-368, 2019. https://doi.org/10.1016/j.energy.2018.12.053.

[8] H. S. Kim, J. H. Kim, and J. Kim, "A review of piezoelectric energy harvesting based on vibration," *Int J. Precis. Eng. Manuf.*, vol. 12, no. 6, pp. 1129-1141, 2011. https://doi.org/10.1007/s12541-011-0151-3.

[9] S. Roundy, P. K. Wright, and J. Rabaey, "A study of low level vibrations as a power source for wireless sensor nodes," *Comput Commun.*, vol. 26, no. 11, pp. 1131-1144, 2003. https://doi.org/10.1016/S0140-3664(02)00248-7.

[10] M. Y. Gao, Y. Wang, Y. F. Wang, and P. Wang, "Experimental investigation of non-linear multi-stable electromagnetic-induction energy harvesting mechanism by magnetic levitation oscillation," *Appl Energy*, vol. 220, pp. 856-875, 2018. https://doi.org/10.1016/j.apenergy.2018.03.170.

[11] S. Adhikari, M. I. Friswell, and D. J. Inman, "Piezoelectric energy harvesting from broadband random vibrations," *Smart Mater. Struct.*, vol. 18, no. 11, Article ID: 115005, 2009. https://doi.org/10.1088/0964-1726/18/11/115005.

[12] Z. Y. Zhou, W. Y. Qin, and P. Zhu, "A broadband quad-stable energy harvester and its advantages over bi-stable harvester: Simulation and experiment verification," *Mech Syst. Signal Process.*, vol. 84, pp. 158-168, 2017. https://doi.org/10.1016/j.ymssp.2016.07.001.

[13] J. Jung, P. Kim, J. I. Lee, and J. Seok, "Nonlinear dynamic and energetic characteristics of piezoelectric energy harvester with two rotatable external magnets," *Int J. Mech Sci.*, vol. 92, pp. 206-222, 2015. https://doi.org/10.1016/j.ijmecsci.2014.12.015.

[14] D. W. Man, D. H. Xu, X. C. Kuang, X. F. Kang, Q. H. Xu, and Y. Zhang, "Analysis of dynamic characteristics of tristable piezoelectric energy harvester based on the modified model," *Math Probl. Eng.*, vol. 2021, Article ID: 3832406, 2021. https://doi.org/10.1155/2021/3832406.

[15] Z. W. Fang, Y. W. Zhang, X. Li, H. Ding, and L. Q. Chen, "Complexification-averaging analysis on a giant magnetostrictive harvester integrated with a nonlinear energy sink," *J. Vib. Acoust. Trans. ASME*, vol. 140, no. 2, Article ID: 021009, 2017. https://doi.org/10.1115/1.4038033.

[16] S. Chiacchiari, F. Romeo, D. M. McFarland, L. A. Bergman, and A. F. Vakakis, "Vibration energy harvesting from impulsive excitations via a bistable nonlinear attachment-Experimental study," Mech Syst. Signal Process., vol. 125, pp. 185-201, 2019. https://doi.org/10.1016/j.ymssp.2018.06.058.

[17] L. Chen, X. Liao, B. B. Sun, N. Zhang, and J. W. Wu, "A numerical-experimental dynamic analysis of high-efficiency and broadband bistable energy harvester with self-decreasing potential barrier effect," *Appl Energy*, vol. 317, Article ID: 119161, 2022. https://doi.org/10.1016/j.apenergy.2022.119161.

[18] P. Kim and J. W. Seok, "Dynamic and energeticcharacteristics of a tri-stable magnetopiezoelastic energy harvester," *Mech. Mach. Theory*, vol. 94, pp. 41-63, 2015. https://doi.org/10.1016/j.mechmachtheory.2015.08.002.

[19] S. X. Zhou, J. Y. Cao, D. J. Inman, J. Lin, S. S. Liu, and Z. Z. Wang, "Broadband tristable energy harvester:

Modeling and experiment verification," *Appl Energy*, vol. 133, pp. 33-39, 2014. https://doi.org/10.1016/j.apenergy.2014.07.077.
[20] S. X. Zhou and L. Zuo, "Nonlinear dynamic analysis of asymmetric tristable energy harvesters for enhanced energy harvesting," *Commun. Nonlinear Sci. Numer Simul.*, vol. 61, pp. 271-284, 2018. https://doi.org/10.1016/j.cnsns.2018.02.017.
[21] D. W. Man, G. Z. Xu, H. M. Xu, and L. P. Tang, "Nonlinear dynamic analysis of bistable piezoelectric energy harvester with a new-type dynamic amplifier," *Comput Intell. Neurosci.*, vol. 2022, Article ID: 7155628, 2022. https://doi.org/10.1155/2022/7155628.
[22] X. Q. Ma, H. T. Li, S. X. Zhou, Z. C. Yang, and G. Litak, "Characterizing nonlinear characteristics of asymmetric tristable energy harvesters," *Mech Syst. Signal Process.*, vol. 168, Article ID: 108612, 2022. https://doi.org/10.1016/j.ymssp.2021.108612.
[23] L. P. Tang and J. G. Wang, "Size effect of tip mass on performance of cantilevered piezoelectric energy harvester with a dynamic magnifier," *Acta Mech.*, vol. 228, no. 11, pp. 3997-4015, 2017. https://doi.org/10.1007/s00707-017-1910-8.
[24] H. F. Liu, W. C. Li, X. W. Sun, C. Cong, C. D. Cao, and Q. Zhao, "Enhanced the capability of magnetostrictive ambient vibration harvester through structural configuration, pre-magnetization condition and elastic magnifier," *J. Sound Vib.*, vol. 492, Article ID: 115805, 2021. https://doi.org/10.1016/j.jsv.2020.115805.
[25] G. Q. Wang, W. H. Liao, B. Q. Yang, X. B. Wang, W. T. Xu, and X. L. Li, "Dynamic and energetic characteristics of a bistable piezoelectric vibration energy harvester with an elastic magnifier," *Mech Syst. Signal Process.*, vol. 105, pp. 427-446, 2018. https://doi.org/10.1016/j.ymssp.2017.12.025.
[26] G. Q. Wang, Y. Ju, W. H. Liao, Z. X. Zhao, Y. Li, and J. P. Tan, "A hybrid piezoelectric device combining a tri-stable energy harvester with an elastic base for low-orbit vibration energy harvesting enhancement," Smart Materials and Structurest, vol. 30, no. 7, Article ID: 075028, 2021. https://doi.org/10.1088/1361-665X/ac057b.
[27] P. Zhu, X. M. Ren, W. Y. Qin, Y. F. Yang, and Z. Y. Zhou, "Theoretical and experimental studies on the characteristics of a tri-stable piezoelectric harvester," *Arch. Appl Mech.*, vol. 87, no. 9, pp. 1541-1554, 2017. https://doi.org/10.1007/s00419-017-1270-9.
[28] H. T. Li, D. Hu, X. J. Jing, W. Y. Qin, and L. Q. Chen, "Improving the performance of a tri-stable energy harvester with a staircase-shaped potential well," *Mech Syst. Signal Process.*, vol. 159, Article ID: 107805, 2021. https://doi.org/10.1016/j.ymssp.2021.107805.